Transmission of Rossby waves through the Philippine Archipelago

Mac Euan D. Malugao[1,2,5], Sen Jan[3], Ming-Huei Chang[3], Tung-Yuan Ho[1,3,4], Yiing Jang Yang[3]

[1] Earth System Science Program, Taiwan International Graduate Program, Academia Sinica, Taipei, Taiwan, R.O.C.

[2] Taiwan International Graduate Program for Earth System Science, National Taiwan University, Taipei, Taiwan, R.O.C.

[3] Institute of Oceanography, National Taiwan University, Taipei, Taiwan, R.O.C.

[4] Research Center for Environmental Changes, Academia Sinica, Taipei, Taiwan, R.O.C.

[5] Department of Marine Science, College of Science and Mathematics, Mindanao State University – Iligan Institute of Technology, Iligan City, Philippines

Corresponding author: Sen Jan (senjan@ntu.edu.tw)

Key Points:

- Satellite altimeter proved Rossby wave transmission through the Philippine archipelago and into central South China Sea.
- Rossby waves entered Celebes Sea and passed Sibutu Passage into Sulu Sea, while β-refracted Rossby wave entered Sulu Sea via Surigao Strait.
- The Mindoro Strait and the Balabac Strait served as gateways for the Rossby waves entering the central South China Sea from the Sulu Sea.

Abstract

Oceanic Rossby waves play a crucial role in shaping the physical and biological dynamics of both open and coastal oceans, especially within the tropical band spanning between the 10°S and 10°N parallels. Yet, the extent to which Rossby waves can transmit and impact the hydrography and ecosystem of semi-enclosed seas like the South China Sea (SCS) remains unclear. This study aims to investigate the transmission of Rossby waves through the Philippine archipelago, using satellite altimeter-derived sea level anomaly (SLA) and coastal tide gauge records. Our findings reveal that westward-propagating Rossby waves in the tropical Pacific Ocean with a wave speed of ~0.64 m s^{-1} first entered the Celebes Sea, and then passed through the Sibutu Passage into the Sulu Sea from April to December 2017. Subsequently, the waves propagated along the northeast coast of Sabah and the east coast of Palawan before exiting through the Mindoro Strait to the central SCS. Additionally, a β-refracted Rossby wave with wave speed of 0.28 m s^{-1} also penetrated the archipelago but at a latitude further north ~10°N from July to November via Surigao Strait and propagated toward the south and north of Palawan, ultimately reaching the west coast of Palawan in the eastern central SCS. This study verifies that the transmission of Rossby waves originating from the east of the Philippines could induce intraseasonal sea level oscillations off Palawan, which could subsequently propagate westward across the central SCS as identified in previous field observations.

Keywords: Sea level anomaly, satellite altimeter, Hovmöller diagram, first baroclinic mode, western boundary

Plain Language Summary

Oceanic Rossby waves are like movers shaping how things work in the world's oceans, especially in tropical bands between 10 degrees south and 10 degrees north of the equator. We wanted to figure out how these waves travel and affect seas like the South China Sea. Using data from satellites and measurements along the coast, we discovered that these waves, traveling at about 0.64 meters per second, first went through the Celebes Sea, then moved through specific passages to reach the Sulu Sea between April and December 2017. Another type of Rossby wave traveled at a different speed through a different route, arriving at the same destination in the South China Sea. This research helps us understand how these waves move through the Philippine islands and impact sea levels around them.

1. Introduction

Large-scale westward-propagating oceanic Rossby waves, which can be identified from sea level anomalies observed by satellites, significantly impact the sea surface height variations, geostrophic current, and hydrography in the ocean and the weather and climate from the atmospheric variations during their journey across the entire basin (Chelton & Schlax, 1996; Jacobs et al., 1993). They transport heat in the meridional direction, regulate the climate, redistribute the water mass and nutrients in the ocean, and shape the ocean circulation (e.g., Anderson & Gill, 1975; Jacobs et al., 1994; Meyers et al., 1996; Stammer et al., 2008; Uz et al., 2001; White et al., 1998). The formation of Rossby waves may originate from wind burst forcing (Anderson et al., 1979; Cabanes et al., 2006; Qiu, 2003), the reflection of Kelvin waves in the eastern boundary (Delcroix et al., 1991; Jacobs et al., 1994; McCreary, 1976), or buoyancy forcing (Piecuch & Ponte, 2012). As Rossby waves approach the western boundary, they can intensify the western boundary current (Anderson et al., 1979; Anderson & Gill, 1975), modulate local sea-level annual cycles (Calafat et al., 2018), and reflect from the western boundary to form Kelvin waves propagating eastward along the equator (du Penhoat & Cane, 1991; White, 2000; Zang et al., 2002). In addition to their importance in ocean dynamics, du Penhoat and Cane (1991) and Spall and Pedlosky (2005) suggested that, as a first mode baroclinic Rossby wave impinges on a small meridional gap in the western boundary, a considerable portion of incident wave energy can transmit through the gap, while wave energy and, in turn, amplitude of reflected Kelvin wave become small, which may have significant impact on the El Niño-Southern Oscillation (ENSO) variability in the Pacific Ocean.

Indeed, a recent study conducted by Jan et al. (2021) observed intraseasonal coastal sea level oscillations off the west coast of Palawan (Fig. 1a and b) and hypothesized that the Rossby waves partially penetrate the islands through Surigao Strait, a conduit between Philippine marginal seas and the western Pacific Ocean at approximately 10°N, into Bohol and Sulu Seas to the west of Palawan, and into central South China Sea (SCS). In addition to influences on the dynamics, the potential penetration of Rossby waves may have substantial ecological impacts in the southern Philippine archipelago via upwelling and mixing of nutrient-rich subsurface waters. For example, Bohol Sea and Sulu Sea are important marginal seas in the Philippines with significant coastal upwelling sites (Cabrera et al., 2011; Villanoy et al., 2011) that support sardine fisheries. Additionally, the penetration of Rossby waves would elevate sea level

variations, amplifying the risk of severe damage during storm surges (Calafat et al., 2018). The potential ecological influences and the increased risk to extreme events warrant a comprehensive understanding of the characteristics of Rossby waves as they impinge on the eastern coasts of the Philippine archipelago from the east.

This study aims to examine the penetration of Rossby wave-induced sea level anomaly signals from the eastern to the western side of the Philippine archipelago and find their pathway and underlying physical processes. The satellite altimeter data and coastal tide gauge records are analyzed to clarify whether the relatively high sea level anomaly (> 0.2 m) observed in the east of the Philippines mainly originates from westward-propagating Rossby waves. Whether the waves could penetrate the southern Philippine islands and reach the SCS is also investigated, particularly for the fourth Rossby wave emanated from the west coast of Palawan observed by Jan et al. (2021). The results obtained from this study is expected to have important implications in many aspects, including climate dynamics, biogeochemical cycling of nutrients, and fisheries management within the Philippine waters.

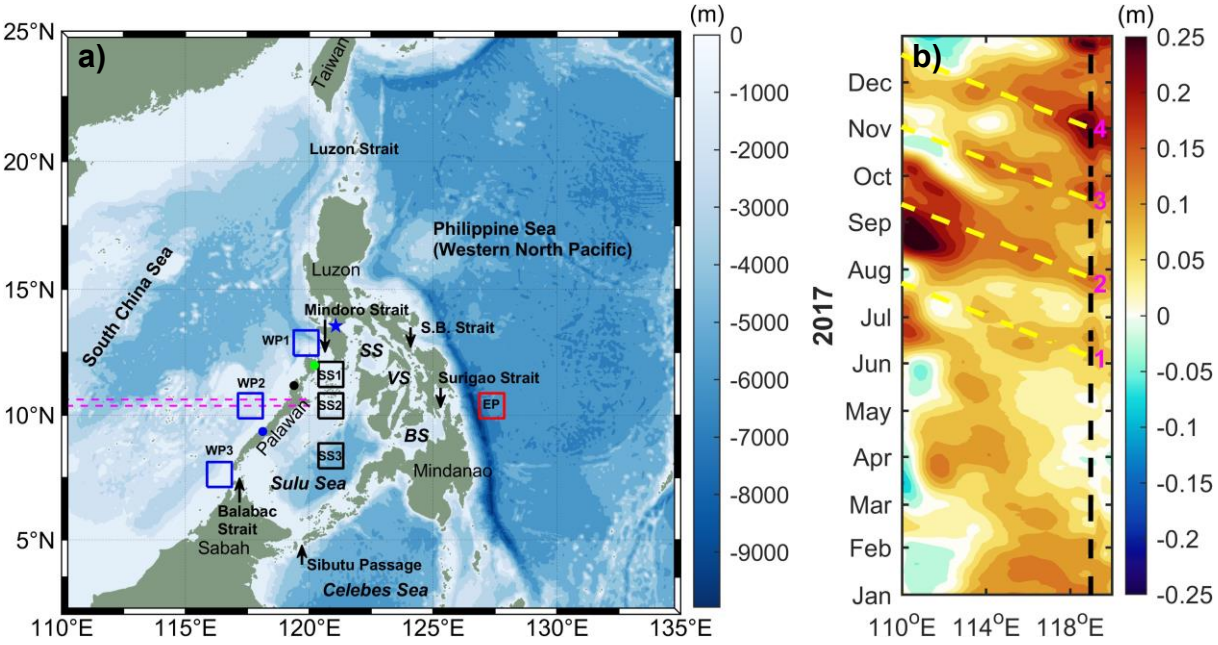

Fig. 1. (a) Bathymetric chart of the Philippine Sea and the South China Sea. Blue, black, and red boxes are the selected sites west of Palawan (WP1, WP2, and WP3), Sulu Sea (SS1, SS2, and SS3), and east of the Philippines (EP), respectively. Coastal tide gauge stations at Coron, El Nido, and Balintang are marked by green, black, and blue dots, respectively. A blue star marks Verde Island Passage. BS, VS, and SS are Bohol Sea, Visayan Sea, and Sibuyan Sea. The rectangle area enclosed by the magenta dashed lines is the meridionally-averaged satellite SLA used for depicting (b). (b) Hovmöller diagram (longitude vs. time) of satellite SLA at 10.5°N (Jan et. al., 2021). The numerals 1–4 mark coastal sea level rise events occurring west of Palawan in 2017. Black dashed line indicates the west coast of Palawan. Yellow dashed lines indicate the westward-propagating SLA signals associated with events 1–4.

2. Data and Methods

2.1 Sea level data

The satellite altimeter-derived Global Ocean Gridded (L4) Sea Surface Heights and Derived Variables Reprocessed provided by the Copernicus Marine Service (available at https://doi.org/10.48670/moi-00148) were collected to identify Rossby waves in the context of sea surface height observations. The satellite-derived sea level anomaly (SLA) data, with a spatial resolution of 0.25° in both the north-south (meridional) and east-west (zonal) directions, was computed by subtracting a 20-year (spanning from 1993 to 2012) mean sea level from the original data covering the period 1993 to 2020. The processed SLAs were specifically examined, particularly the year 2017, to validate the hypothesis raised by Jan et al. (2021) regarding the penetration of Rossby waves through the Philippine islands. Sea level data recorded at three coastal tide gauge stations (refer to Fig. 1b for their locations) were acquired from the National Mapping and Resource Information Authority of the Philippines (https://www.namria.gov.ph) to enhance the associated analysis.

2.1 Methodology

Whether a westward-propagating SLA signal can extend to the west of Palawan and into the Philippine marginal seas, particularly in the Sulu Sea is the key to examine the transmission of the signal through the Philippine islands. Time series of area-averaged daily SLA at seven selected rectangles (Fig. 1a) are prepared for this purpose. Three of the seven selected sites are located west of Palawan within the rectangle of 12.375°–13.375°N and 119.375°–120.375°E (WP1), 9.875°–10.875°N and 117.125°–118.125°E (WP2), and 7.125°–8.125°N and 115.875°–116.875°E (WP3). The three sites located in the Sulu Sea are within the rectangle of 11.125°–12.125°N and 120.375°–121.375°E (SS1), 9.875°–10.87°N and 120.375°–121.375°E (SS2), and 7.875°–8.875°N and 120.375°–121.375°E (SS3). The last site is located east of the Philippines (EP) bounded by 9.875°–10.875°N and 126.875°–127.875°E. The linear least-square fit of the area-averaged daily SLA time series was subtracted from the original time series (Fig. 2a) to eliminate trends in the data. In the tide-gauge station recorded sea levels, the data at Balintang contains missing data (blue line in Fig. 2b), therefore a harmonic analysis based on Godin (1972) and Foreman (1977, 1978) with the application of a MATLAB package T_Tide (Pawlowicz et

al., 2002) was used to compute the harmonic constants of the tidal sea levels at this station. The harmonic constants are subsequently used to composite the tidal sea level during the missing data period. Similar detrend method is applied to the tidal sea level records at the three Palawan stations.

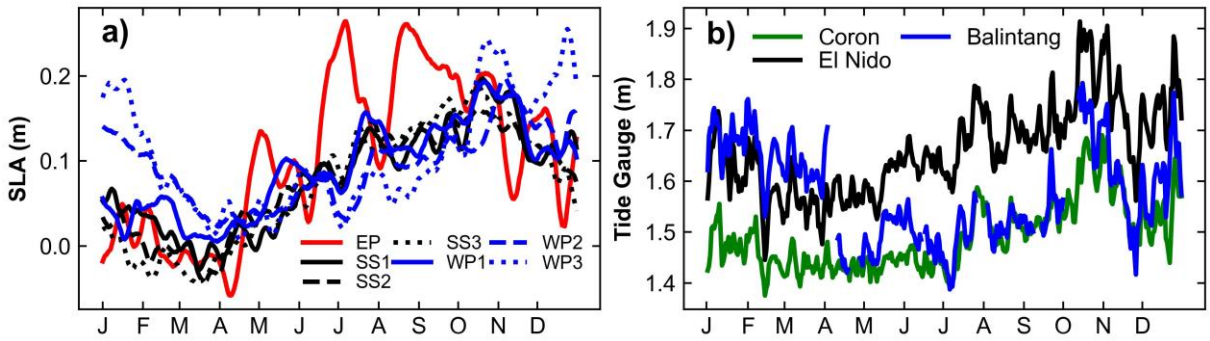

Fig. 2. (a) Time series of area-averaged daily SLA of the seven selected sites. (b) Time series of daily-averaged tide-gauge sea level records at the three Palawan stations.

The analysis involved examining monthly mean SLAs across the subtropical and tropical Pacific Ocean, spanning from 25°S to 25°N and from 110°E to 70°W. Signals of considerable magnitude, with absolute values > 0.2 m, were the focus of this analysis. A spatial low-pass filter achieved by an area mean of every 9 × 9 grids was applied to remove high-wavenumber features from the SLA maps (Fig. 3a–h). A Hovmöller diagram is plotted using the monthly mean SLA, meridionally averaged between 4.875° and 5.625°N, spanning across the Pacific Ocean from 110°E to 70°W (Fig. 4a). The linear propagation speed of the SLA signal is estimated from the slope of each SLA signal (yellow dashed line in Fig. 4a). A wavelet power spectrum using Morlet wavelet is plotted using a 5-year (2015–2019) daily SLA average within the range of 4.875°–5.625°N and 130°E–80°W (Fig. 4b) following the method of (Torrence & Compo, 1998).

To quantify the characteristics of the Rossby waves, a wavenumber-frequency spectrum similar to the computation and illustration presented in Jan et al. (2021) is generated using a 20-year (2001–2020) daily SLA time series. The zonally SLA time series, spanning from 130°E to 80°W, is the SLA average within the latitudinal band of 4.875° to 5.625°N (Fig. 4c and d). The dispersion relation of Rossby waves (red, yellow, and blue dashed lines in Fig. 4c and d) is computed using the equation (Cushman-Roisin, 1994),

$$\omega = -\beta_0 R^2 \frac{l}{1+R^2(l^2+m^2)},$$

where β_0 is the Rossby parameter defined as $\beta_0 = 2\Omega \cos\varphi\, a^{-1}$ (Ω is the angular velocity of the earth's rotation 7.2921×10^{-5} rad s^{-1}, φ is the latitude 5°N here, and a is the earth's radius 6371 km), R is the Rossby radius of deformation, and l and m are zonal and meridional angular wavenumbers, respectively. The theoretical zonal phase speed (white lines in Fig. 4c and d) was calculated using $C_x = \omega / l$. The dispersion relation for baroclinic Rossby radius of deformation R 180, 215, and 260 km, is overlaid on the spectrum. The three radii are based on the globally computed first baroclinic Rossby radius of deformation climatology (Chelton et al., 1998) mean (±1 standard deviation) within the range of 4.5°–5.5°N and 130°E–80°W 215.3±28.8 km. The wavenumber-frequency spectrum is used to examine the estimated Rossby wave speed and detect westward propagating SLA energy signals corresponding to that of the theoretical first baroclinic Rossby wave.

To detect the oscillation in an annual cycle, which is a characteristic of first baroclinic Rossby waves from 4°–6°N (Kessler, 1990; G. Meyers, 1979; Zang et al., 2002), the detrended SLA time series and tidal sea level records are low-pass filtered by applying a Butterworth filter with a cutoff frequency of 5.7870×10^{-8} cps (equivalent to 200-day period) to the time series data (Fig. 5a and b). To have a temporal and spatial view of the results obtained from Fig. 5b, the daily SLA in each grid ranging between 0°–15°N and 110°–130°E was detrended and low-pass filtered as the aforementioned procedure, and plotted as monthly mean as illustrated in Fig. 6a–i. Furthermore, a 30-day low-pass filter with a cutoff frequency of 3.8580×10^{-7} cps was applied to the detrended SLA time series and tidal sea level records. This processed SLA time series is used to clarify whether the observed SLA signal (> 0.2 m) at 10.5°N east of the Philippines in Jan et al. (2021) was from a Rossby wave (Fig. 7a–d). The potential route of the Rossby wave penetration is also investigated. The monthly mean of low-pass-filtered SLAs within 0°–15°N and 110°–180°E are depicted in Fig. 8a–j.

3. Results and Discussion

3.1 Westward-propagating SLA signals

Fig. 3 shows the low-pass filtered monthly mean SLA over the tropical and subtropical Pacific Ocean. The filled blue (yellow) square and circle mark the center of the positive and negative SLA signals, respectively, in the northern (southern) hemisphere. The black (blue)

dashed line marks 5°N (6°S). Throughout the year 2017, noticeable basin-scale westward-propagating positive and negative SLA signals were observed within the tropical Pacific band ranging from 10°N to 10°S in both the northern and southern hemispheres. These SLA patterns exhibit spatial and temporal characteristics consistent with Rossby waves, a finding supported by analyses of satellite sea surface height observations (e.g., Chelton & Schlax, 1996; Zang et al., 2002) and numerical model simulations (Fu et al., 1991; Spall & Pedlosky, 2005).

At 160°E (Fig. 3a), the positive SLA (crest) signifies downwelling, while at 165°W (Fig. 3d), the negative SLA (trough) indicates upwelling, which are the indicative pattern of Rossby wave (Uz et al., 2001). These crest or trough pairs center around 5°N and 6°S, symmetrically positioned concerning the equator. This alignment corresponds to the characteristic behavior of the theoretical first meridional mode Rossby wave, initially proposed by Matsuno (1966) and also agrees findings reported by Chelton and Schlax (1996), Delcroix et al. (1991), and Zang et al. (2002), who utilized satellite-derived observations. Notably, Zang et al. (2002) observed Rossby waves at 6°N and 6°S using TOPEX/Poseidon data spanning 1992–2000, differing slightly from our findings of 5°N in the northern hemisphere. This difference in observed Rossby wave locations may be attributed to variations in wind forcing. Kessler (1990) utilized bathythermograph profiles in the northern tropical Pacific from 1970 to 1987 and found a close resemblance between the amplitude pattern of wind stress curl, capable of generating Rossby waves via Ekman pumping, and the depth of the 20°C isotherm (a proxy for sea surface height). This similarity was particularly pronounced near 5–6°N, lending support to the observed location of the Rossby wave noted by Zang et al. (2002) and this study. It is also worth noting that a robust El Niño event occurred in 2015–2016, evidenced by the Ocean Niño Index (ONI) reaching as high as 2.6 (NOAA/National Weather Service, 2023) prior to 2017. Given that Rossby waves can manifest as a reflection of Kelvin waves upon reaching the eastern boundary of the Pacific Ocean during El Niño events (Delcroix et al., 1994, 1991; Jacobs et al., 1994; Kessler, 1990; McCreary, 1976), it is plausible that the Rossby wave observed in 2017 could have originated from the 2015–2016 El Niño event.

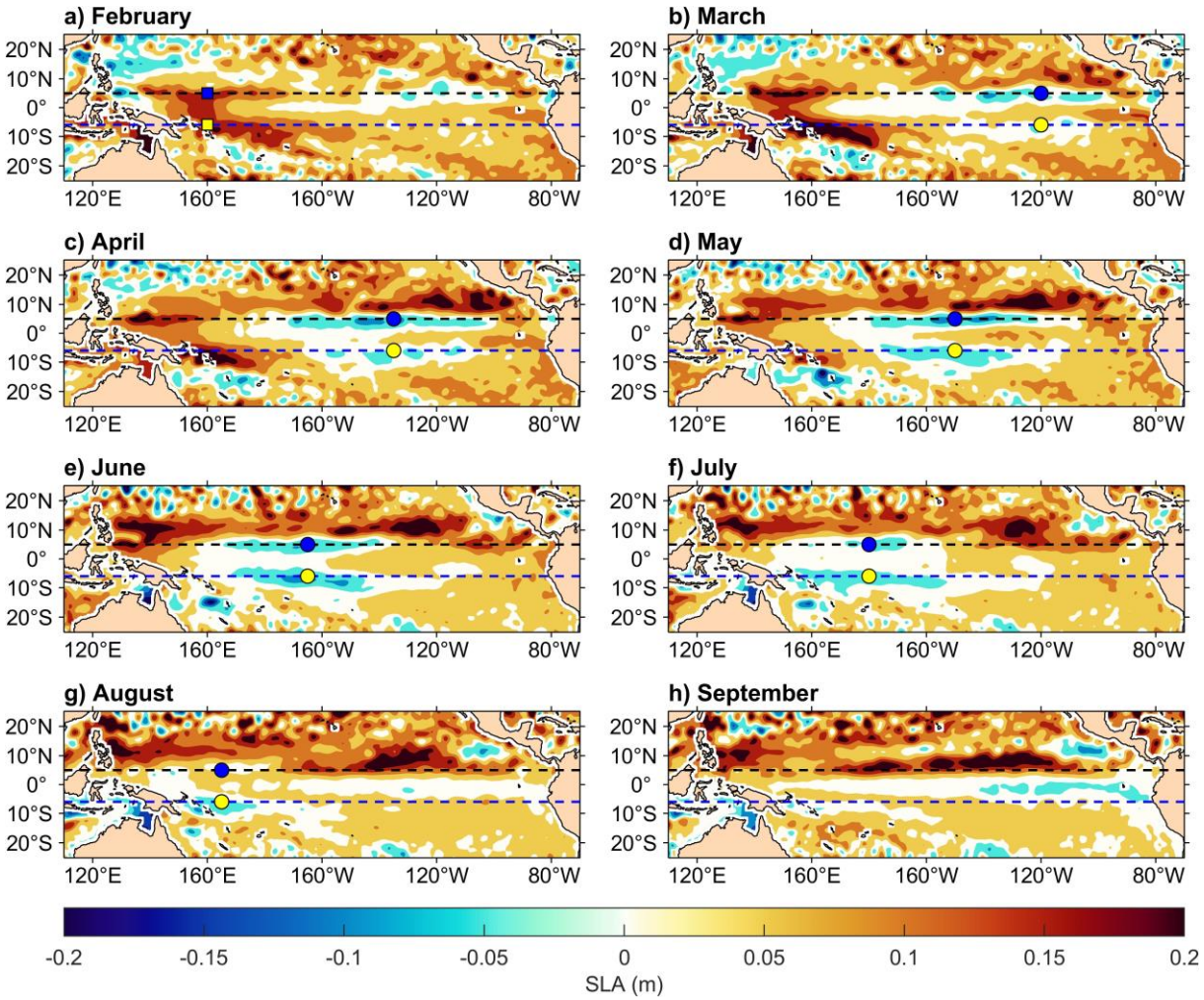

Fig. 3. Low-pass filtered satellite SLA in the subtropical and tropical Pacific Ocean. In the northern hemisphere (southern hemisphere), the filled blue (yellow) square and circle denote the centers of positive and negative SLA signals, respectively. The black dashed line represents 5°N, while the blue dashed line represents 6°S.

The monthly mean SLA depicted in Fig. 4a serves as the basis for calculating the phase speed of Rossby waves. These low-latitude SLA patterns observed in the northern hemisphere are anticipated to reach the east coast of the Philippines. Note that our analysis focuses on the prominent SLA signal, which manifests as a trough, indicated by the filled blue circles in Fig. 3b–g. In the case of the crest, it had already translated halfway in the western boundary by April 2017 (Fig. 3c), while the trough apparently propagated westward from March to July (Fig. 3b–f). The slope of the yellow dashed line in Fig. 4a corresponds to the phase speed of the Rossby wave, 0.64 m s^{-1}, at approximately 5°N. The wavelength of the Rossby wave is also estimated from Fig. 4a. The propagating distance of the crest between March and April (30 days) covered

15 degrees of longitude, marked by the filled yellow triangles in Fig. 4a, without considering potential influences from a western boundary. In March, the Rossby wave crest and trough were located at approximately 145°E and 120°W, respectively, which suggests a half wavelength of ~10,545 km. Consequently, the estimated wavelength is 21,090 km. The associated period estimated from Fig. 4a is approximately 12 months. Furthermore, from the wavelet power spectrum of SLA in Fig. 4b illustrates SLA energy predominantly in 2017, with a period of 360 days.

The wavenumber-frequency spectrum depicted in Fig. 4c reveals the presence of energy attributed to a basin-scale westward-propagating SLA with an annual period. This energy aligns closely with the dispersion relation computed using baroclinic Rossby radii of 180 km (illustrated by the red dashed line) and 260 km (shown as the blue dashed line) in Fig. 4c. Upon magnifying the area enclosed by the black rectangle in Fig. 4d (corresponding to Fig. 4c), the period associated with relatively low SLA energy (enclosed by the black oval) falls within the range of 350 to 360 days. The SLA energy, close to the dispersion relation computed with a 180 km radius of deformation, exhibits a theoretical phase speed of approximately -0.7 m s^{-1} (the negative sign implies westward propagation) and a wavenumber of approximately -4.5×10^{-8} m^{-1} (or ~22,000 km). These values are comparable to the characteristics of the Rossby wave observed in 2017. These findings are consistent with those reported by Kessler (1990) of a Rossby wave near 5°N which exhibited an annual period, a zonal wavelength of ~23,000 km (model estimate ~21,000 km), and a model-derived phase speed of ~0.67 m s^{-1}.

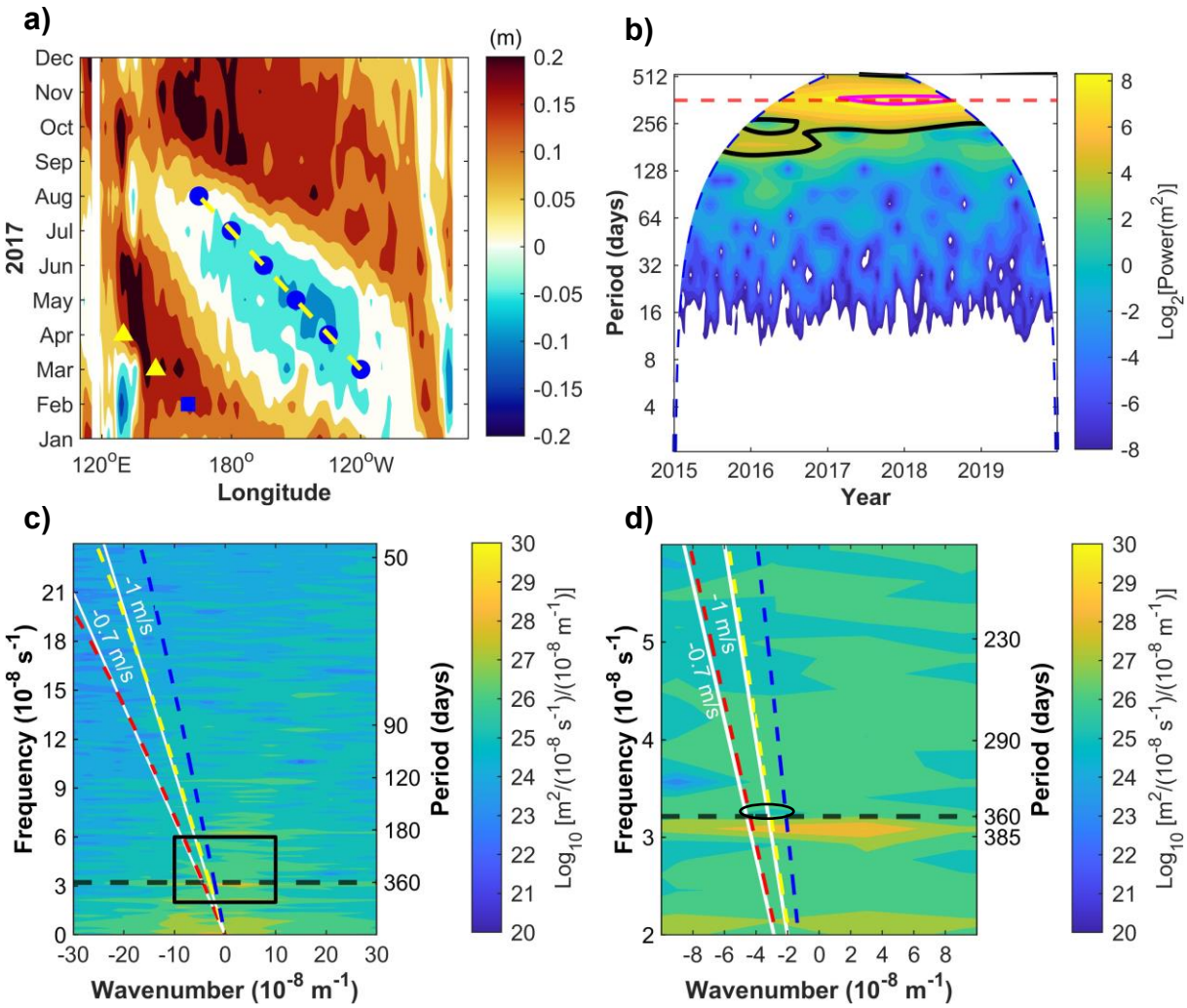

Fig. 4. (a) Hovmöller diagram illustrating satellite-derived SLA centered at 5°N. The filled blue square and circle correspond to those in Fig. 2a–g. The filled yellow triangles denote the crest centers in March and April, with the yellow dashed line indicating the phase speed of the westward-propagating negative SLA signal. (b) Wavelet power spectrum normalized by corresponding variance (σ^2=0.0015 m^2) .The blue dashed line indicates the cone of influence. The red dashed line denotes the 360-day period. Magenta contour is the SLA energy with approximately annual period. Black contour indicates the region with greater than 95% confidence level. (c) Wavenumber-frequency spectrum of satellite SLA. The red, yellow, and blue dashed lines are dispersion relations computed using *R* of 180, 215, and 260 km, respectively. The white lines show the computed theoretical phase speeds of −0.7 and −1 m s^{-1}. The horizontal black dashed line marks 360 days. (d) A close-up of the black rectangle in (c), where the black oval indicates westward-propagating (negative wavenumber) SLA energy with periods within 350 and 360 days.

3.2 Penetration of SLA signals through the Celebes Sea

Fig. 5 shows detrended and 200-day low-pass filtered satellite SLA time series off the eastern Philippines (red line), in the Sulu Sea (black lines), and off the west coast of Palawan (blue lines). In Fig. 5a, detrended and 200-day low-pass filtered sea level data from tide gauge stations (cyan lines) are presented for comparative analysis. The low-frequency sea level variations observed at WP2 (blue dashed line) and WP3 (blue dotted line) off the west coast of Palawan show significant correlation with those recorded at Balintang (cyan dotted line), exhibiting Pearson's correlation coefficients of 0.90 and 0.95, respectively. Moreover, WP2 exhibits a strong correlation with sea level variations at Coron (cyan line) and El Nido (cyan dashed line), with correlation coefficients of 0.97 and 0.88, respectively. This finding suggests that the satellite-derived SLA within these specific areas can effectively serve as a proxy for understanding coastal sea level variations along the west coast of Palawan.

Further to the north, the low-frequency sea level variation at WP1 (blue line) and SS1 (black line) show relatively weak (correlation coefficient 0.36) and moderate (correlation coefficient 0.60) correlations, respectively, with those observed at Coron (cyan line). Importantly, the low-frequency sea level variation at SS1 exhibit a notably high correlation (correlation coefficient 0.90) with El Nido (cyan dashed line). This finding supports that the long-term variability of SLA at the major passage connecting the Sulu Sea and the SCS, the Mindoro Strait, can be effectively assessed using satellite altimeter data. Therefore, the analysis of detrended and low-pass filtered satellite-derived SLA proves pivotal in examining the potential penetration of Rossby waves and understanding their probable pathway.

Fig. 5b shows that a quasi-annual sea level oscillation with period > 330 days extending from February to December 2017 is clearly observed at WP2 and WP3. At WP2, the crest higher than 2 cm (filled red) appears during April–May, while a trough lower than −2 cm (blue shading) is noticeable during August and October. A similar pattern can be observed at WP3 but with relatively higher amplitude (> 3 cm for crest and < −3 cm for trough).

The annual variation of SLAs at SS2 and SS3 in the Sulu Sea have similar magnitudes to that at WP1 with a crest approximately 1 cm (green shading) and a trough lower than −2 cm (magenta shading) around March–April and July, respectively. Note that SS1 has relatively higher amplitude with a crest higher than 1 cm (brown shading) in April and a trough lower than −3 cm (yellow shading) in August. The low-frequency satellite SLA at EP does not exhibit a

similar oscillatory pattern observed in the 2017 Rossby wave observed at ~5°N. This is presumably due to the more northly location of EP (~10°N), affecting the distinctive characteristics observed at this latitude.

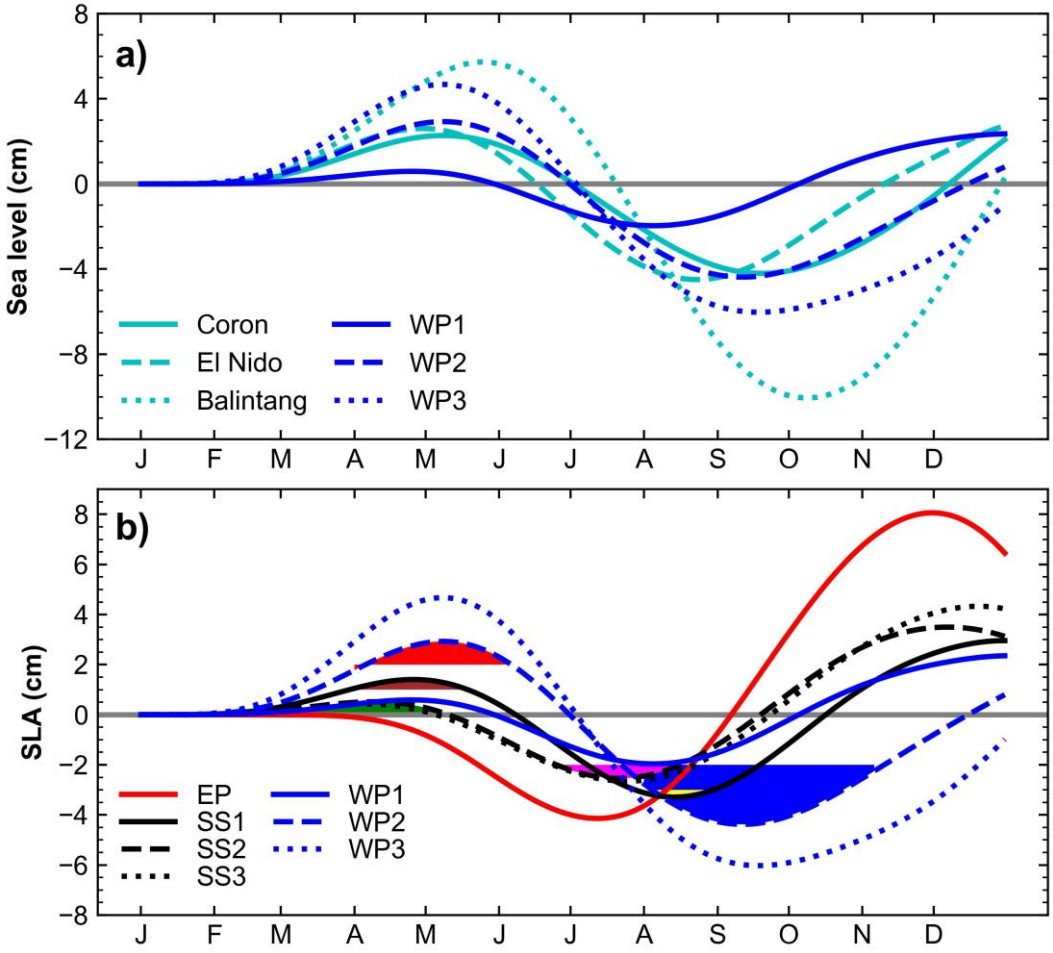

Fig. 5. (a) Time series of detrended and 200-day low-pass filtered satellite SLA and tide gauge station recorded sea levels west and north of Palawan. (b) Detrended and 200-day low-pass filtered satellite SLA across Philippines. Red and blue shadings indicate satellite SLA greater than 2 cm and lower than −2 cm, respectively, at WP2. Green and magenta shadings are satellite SLA smaller than 1 cm and lower than −2 cm, respectively, at SS2 and SS3. Brown and yellow shadings are satellite SLA greater than 1 cm and lower than −3 cm, respectively, at SS1.

The cross-correlation (correlation coefficient r_{SLA}) of the low-frequency satellite SLA between SS2 and EP is 0.96 at zero-lag. At WP2 and SS1, WP2 and SS2, and WP2 and WP1, the r_{SLA} is 0.77 at a 27-day lag, 0.51 at a 54-day lag, and 0.63 at a 37-day lag, respectively. Analyzing the variability of the low-pass filtered SLAs in Fig. 5b reveals that the crest (green

shading) and trough (magenta shading) occurrences in the northern Sulu Sea (SS2) lead those off the west coast of Palawan at WP2 (red and blue shading in Fig. 5b) by 54 days.

This result suggests that the SLA oscillation at WP2 could be sourced from the northern Sulu Sea via the Mindoro Strait. The lagged correlation between EP and SS2, however, suggests that no physically plausible SLA signal penetrated from the east of the Philippines through the Surigao Strait (see its location in Fig. 1a) to the Sulu Sea (SS2). The most plausible entrance of the associated SLA signal is the Sibutu Passage (Fig. 1a), which connects the Celebes and Sulu Seas. Results from the lagged cross-correlation analysis further suggest that, after entering Sibutu Passage, the low-frequency SLA oscillation moved from SS2 to SS1 toward the Mindoro Strait in the Sulu Sea. After passing through the Mindoro Strait into the central SCS, the coherent SLA signal moved southward along the west coast of Palawan.

The pathway of the transmitted SLA signal is examined using the low-pass filtered satellite SLA around the Philippine archipelago (Fig. 6a–i). In March 2017, positive SLA of approximately 2 cm appeared off the west coast of Palawan, in the Sulu Sea, and the southern part of the Celebes Sea (Fig. 6a). The positive SLA continuously increased to greater than 2 cm in these regions and northeast of Sabah in April and May (Fig. 6b and c). As time progressed to June, the SLA along the east and northern half coast of Palawan decreased to smaller than 2 cm, while the southern half coast of Palawan and the southern Celebes Sea remained larger than 2 cm (Fig. 6d). The SLA eventually diminished in July (Fig. 6e). The SLA pattern dramatically reversed from positive to negative in August (Fig. 6f). Thereafter the SLA over these regions remained negative until November (Fig. 6g–i).

The aforementioned results suggest that the penetration of the 2017 Rossby wave is plausible, particularly for the SLA crest. It indicates that the Rossby wave transmitted into the Celebes Sea at about 5°N in March (Fig. 3b). As the Rossby wave further entered the Sulu Sea through the Sibutu Passage, it went along the northeast coast of Sabah and the east coast of Palawan through Mindoro Strait and between Coron and El Nido. After the SLA signal passed the Mindoro Strait to the SCS, SLA signal extended to the west coast of Palawan (Fig. 6d). Note that a relatively higher SLA signal (> 4 cm) appeared south of Palawan, which suggests that the SLA signal could also transmit through the narrow and shallow Balabac Strait. It is also noticed that the SLA signal (> 2 cm) expanded to the Makassar Strait connecting the Celebes Sea and the Java Sea (Fig. 6c), which is indicative of the Rossby wave transmitting toward the Indonesian

marginal seas as well as the Indian Ocean (du Penhoat and Cane, 1991; Spall and Pedlosky, 2005). The temporal and spatial patterns of the negative SLA signal (Rossby wave trough in Fig. 6f–i) are similar to those of the positive SLA signal.

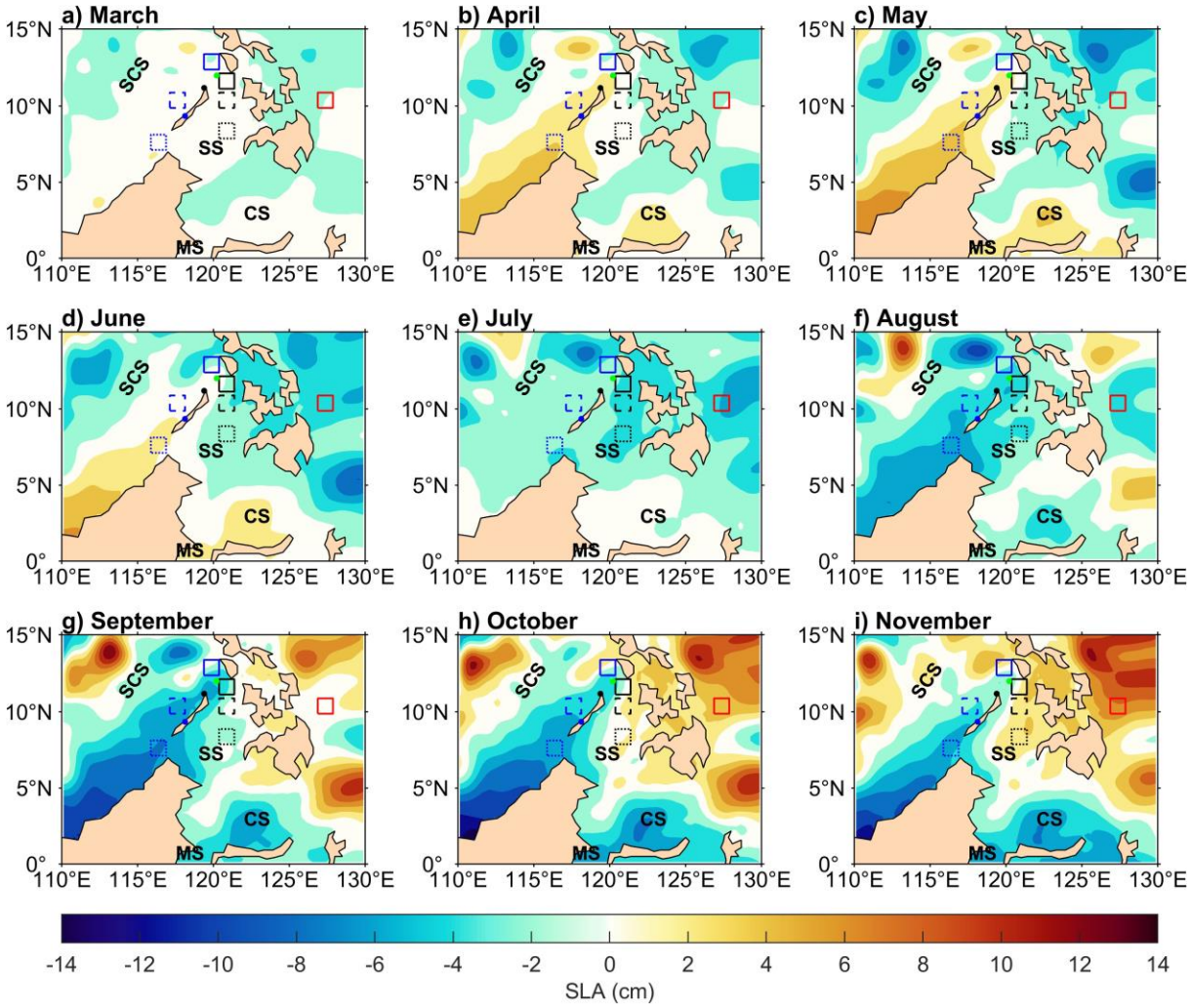

Fig. 6. Monthly mean of temporal and spatial variation in detrended and 200-day low-pass filtered satellite SLA around the Philippines. The color and line style of the rectangles correspond to those in Fig. 4b. CS means Celebes Sea, SS represents Sulu Sea, SCS represents South China Sea, and MS stands for Makassar Strait.

3.3 Penetration of SLA signals through Surigao Strait

Fig. 7 shows the detrended and 30-day low-pass filtered satellite SLA and tide gauge record time series. In the west of Palawan, this processed SLA at WP2 (blue dashed line) and WP3 (blue dotted line) are highly correlated with that at Balintang (cyan dotted line) and their correlation coefficients are 0.70 and 0.82, respectively, as the processed SLA at WP1 (blue line)

311 is highly correlated with that at El Nido (cyan dashed line) with a correlation coefficients of 0.75.
312 In the northern part of Sulu Sea, the SLA at SS1 (black line) is highly correlated with the tide
313 gauge sea level at Coron (cyan line) and El Nido (cyan dashed line), and the correlation
314 coefficients are 0.75 and 0.90, respectively. Fig. 7b–d show the SLA time series east of
315 Philippines (EP), Sulu Sea (SS1–SS3), and west of Palawan (WP1–WP3). Noticeable peaks with
316 the processed SLA greater than 10 cm appeared in the middle of July and early September 2017
317 at EP. In the Sulu Sea, SLA peaks (4–6 cm) appeared in early August and early November. West
318 of the Palawan, SLA peaks (6–10 cm) were also in early August (at WP1 only) and early
319 November (at WP1 and WP3), whereas SLA peaks at WP2 (2–6 cm) appeared in mid-August
320 and late November, which are approximately 10 days behind that of WP1. The period of
321 significant SLA oscillation (amplitude > 10 cm) at EP was during July and October (thick
322 vertical black dashed lines in Fig. 7b–d). Whereas at SS1, SS2, andWP1, the period was from
323 August to November. Additionally, significant SLA oscillation at WP2 (thin vertical black dash
324 lines in Fig. 7d), was from early August to early December, which is approximately 10 days after
325 that at SS1, SS2, and WP1.

326 The r_{SLA} of satellite SLA at SS1, SS2, and SS3 versus that of EP are 0.66 at 20-day lag,
327 0.70 at 20-day lag, and 0.73 at 15-day lag, respectively. The r_{SLA} between WP2 and WP1, SS1,
328 and SS2 is 0.60 at 10-day lag, 0.70 at 8-day lag, and 0.41 at 16-day lag, respectively. These
329 suggest that the associated SLA signal at EP leads that in the Sulu Sea, and the signal in the Sulu
330 Sea leads that off west of Palawan at approximately 20 and 10 days, respectively. The period of
331 significant SLA oscillations and lagged correlations suggest that the SLA off the eastern
332 Philippines leads that in the Sulu Sea and in turn the west of Palawan, particularly at WP2.

333 The aforementioned SLA analysis supports the hypothesis proposed by Jan et. al. (2021),
334 which suggests the penetration of Rossby waves through the Philippine archipelago to the Bohol
335 and Sulu Seas and exiting Mindoro Strait (WP1) and Balabac Strait (WP3) to the west of
336 Palawan (WP2). The Rossby waves eventually emanated from the west coast of Palawan
337 propagating westward in the central SCS. This could be the source of the fourth intraseasonal
338 velocity and satellite oscillations off Palawan and explains the weak correlation of the fourth
339 event of southwesterly monsoon strengthening during early October 2017 and the SLA rise along
340 the west coast of Palawan in November (Jan et al., 2021).

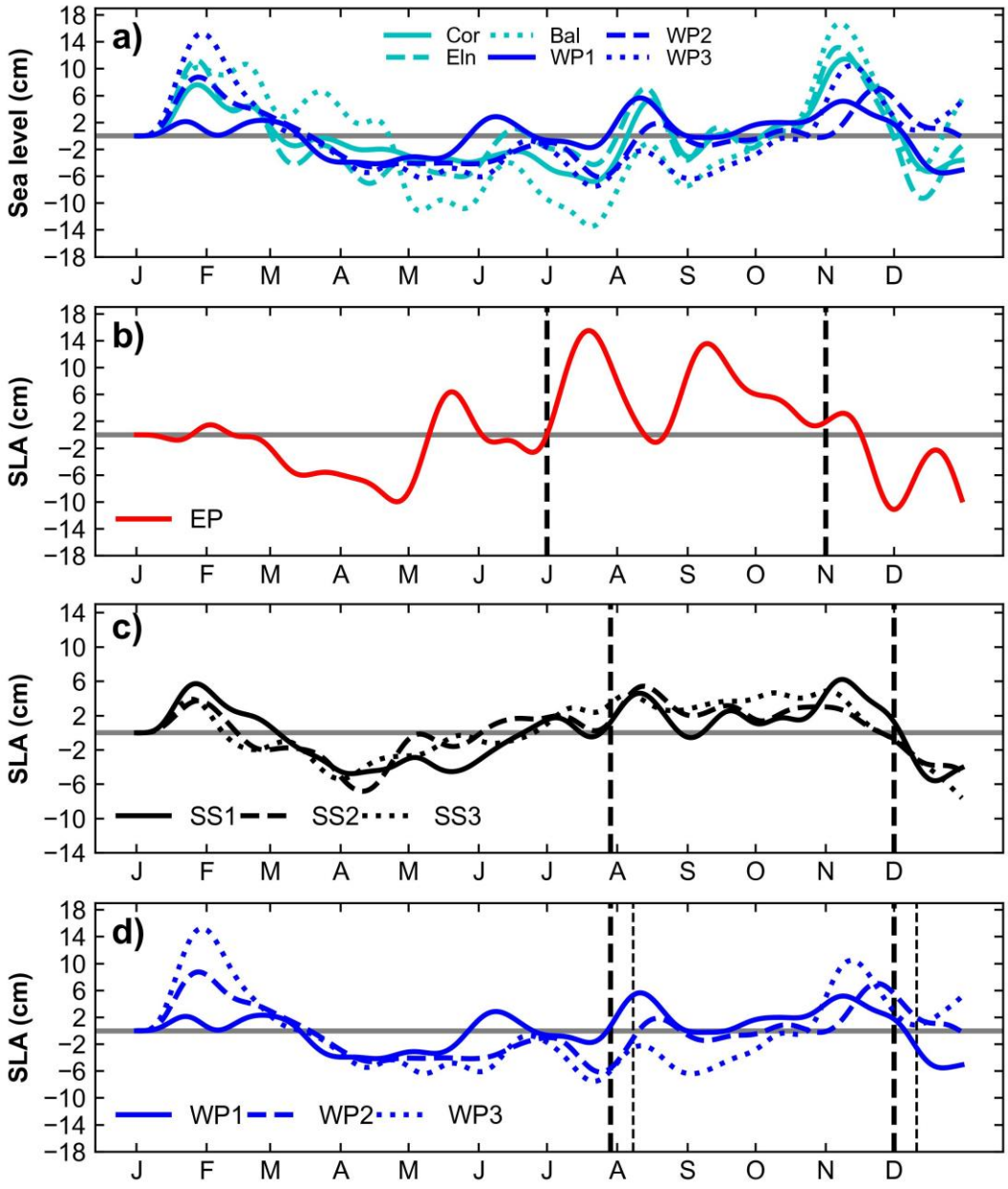

Fig. 7. (a) Time series of detrended and 30-day low-pass filtered satellite SLA alongside tide gauge station recorded sea levels west and north of Palawan. Detrended and 30-day low-pass filtered satellite SLA at (b) EP, (c) S1–S3, and (d) WP1–WP3. Thick vertical black dashed lines indicate the duration of positive SLA signal (crest). Thin vertical black dashed lines indicate the duration of positive SLA signal (crest) in WP2.

341 The peaks in the SLA variations observed east of the Philippines is verified using the
342 temporal and spatial variations of processed SLA from the SCS to the 180°E (Fig. 8a–j). The
343 westward-propagating positive and negative SLA signals at approximately 5°N impinged on the
344 western boundary from April to October (Fig. 8b–h). These SLA signals observed in Fig. 3a–g

are verified as the first baroclinic Rossby wave, which penetrated the southern Philippine archipelago (Fig. 6) and induced a quasi-annual oscillation off the west coast of Palawan (Fig. 5). Between approximately 10° and 15°N, westward-propagating positive and negative SLA signals impinged on the western boundary from July to December (Fig. 8e–j). These SLA signals show characteristics of beta-refracted Rossby waves as those observed by Chelton and Schlax (1996) and Jacobs et al. (1994). The beta-refracted Rossby waves are generated by the reflection of Kelvin waves along the eastern boundary (Jacobs et al., 1994; Sirven et al., 2019). In the case we analyzed, the boundary is the western coastlines of the central and north America. The wave speed estimated using time-longitude plot of detrended and 30-day low-pass filtered daily SLA centered at 10.5°N (i.e., 10.375°–10.625°N average) from 130°E–180° is approximately 0.28 m s^{-1} (Figure S1), which is comparable to the first mode of baroclinic Rossby waves wave speed 0.2–0.3 m s^{-1} at about 10.5°N obtained from the theory (Chelton and Schlax, 1996) and the observation (Jan et al., 2021).

The possible pathways of the beta-refracted Rossby wave crest transmitted across the Philippine archipelago is examined using Fig. 8e–i. In July (Fig. 8e), the crest impinged on the eastern Philippines, which resulted in a SLA peak greater than 10 cm east of the Philippines (Fig. 7b), and entered the Surigao Strait (see Fig. 1a). One month later, in August (Fig. 8f), the crest progressed into the Sulu Sea via Bohol Sea and into the northern Palawan via Bohol Sea, Visayan Sea, Sibuyan Sea, and Mindoro Strait, as shown by the simultaneous peaks of approximately 6 cm at S1–S3 (Fig. 7c) and WP1 (Fig. 7d). Subsequently, this SLA peak moved toward WP2 with approximately 2 cm height 10 days after passed WP1 (Fig. 7d). The 2 cm peak at WP2 propagated westward, contributed to the second event (Fig. 1b) observed by Jan et al. (2021), and consequently resulted in a decrease in SLA at WP2 (Fig. 8g and 7d) in September. The trailing crest continued to propagate toward WP2 in October (Fig. 8h) and November (Fig. 8i). In November, the SLA crest (Fig. 8i) apparently passed WP1 (Mindoro Strait) and WP3 (Balabac Strait) led to a 6 cm and 8 cm peaks in early November (Fig. 7d), respectively. This SLA signal eventually reached WP2 (Fig. 7d) and further propagated westward as the fourth event in Fig. 1b (Jan et al., 2021). Note that the Rossby wave crest (Fig. 8e–g) at approximately 13°N could also pass San Bernardino Strait (S.B. Strait in Fig. 1a), Sibuyan Sea, and exit Mindoro Strait and Verde Island Passage (blue star in Fig. 1a).

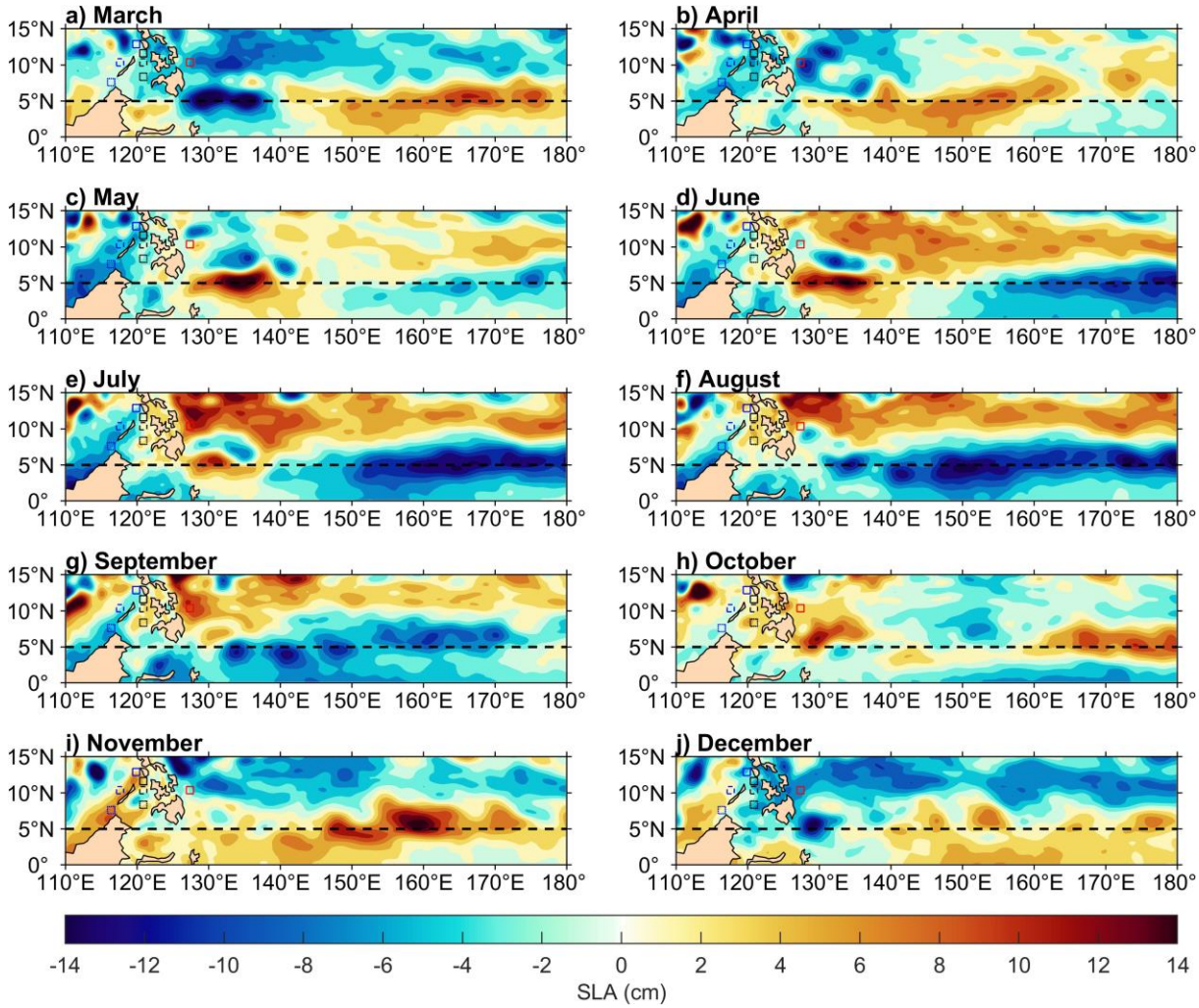

Fig. 8. Monthly temporal and spatial variations in detrended and 30-day low-pass filtered satellite SLA. The color and line style of the rectangles correspond to those presented in Fig. 7b–d.

4. Conclusions

The examination of satellite-derived SLA data, combined with sea level information gathered from fixed tide gauge stations along the Philippine coasts, delineated the westward propagation of first baroclinic Rossby waves within the tropical Pacific Ocean. This analysis revealed these waves' potential to transmit the southern Philippine archipelago and penetrate into the SCS. The estimated wave speed for the Rossby wave is approximately 0.64 m s^{-1}, exhibiting a wavelength of ~21,000 km and a yearly period. This wave speed is comparable to that of the Rossby waves at about 5°N, which is 0.7 m s^{-1} obtained from the theory and ~0.67 m s^{-1} derived from the numerical simulation (Kessler, 1990).

Notably, among the Rossby waves detected from satellite SLA data between 2015 and 2019, the 2017 Rossby wave emerged as the most prominent. This particular Rossby wave translated westward along 5°N, reaching the western boundary of the North Pacific before entering the Celebes Sea and proceeding into the Sulu Sea via the Sibutu Passage. The indicative SLA signal of the Rossby wave hugged the northeast coast of Sabah and east coast of Palawan, and passed through the Mindoro Strait and the passage between Coron and El Nido to the west of Palawan. As the schematic shown in Fig. 9, the Rossby wave also passed the Makassar Strait, potentially extending its influence into the Indian Ocean.

The temporal progression of the SLA around the Mindoro Strait also suggests that a pair of cyclonic and anticyclonic eddies could be generated when the flow generated by the Rossby wave passed westward through the Mindoro Strait. In addition to these findings, a β-refracted Rossby wave, positioned at approximately 10.5°N, is observed with wave speed of 0.28 m s^{-1}, which is close to the theoretical speed of 0.25 m s^{-1} (Chelton & Schlax, 1996) and observed speed of 0.2–0.3 m s^{-1} (Jan et al., 2021). The crest of this β-refracted Rossby wave impinged on the east coast of the Philippines and penetrated through the archipelago through the Surigao Strait. As illustrated by Fig. 8, two pathways toward west of Palawan are observed: one directed southward to the Bohol Sea, Sulu Sea, and Balabac Strait and the other translated northward to the Bohol Sea, Visayan Sea, Sibuyan Sea, and Mindoro Strait of Palawan island.

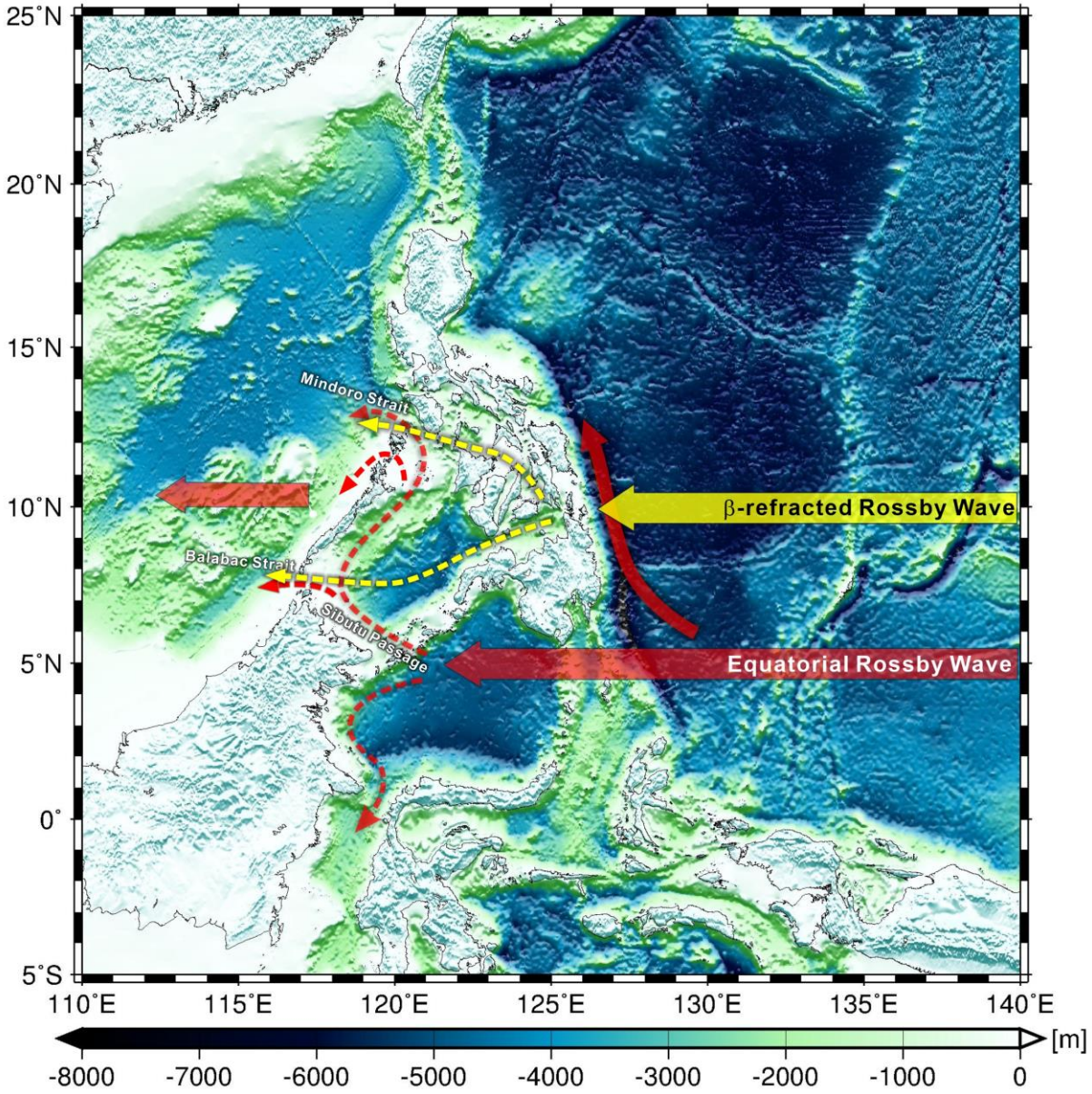

Fig. 9. A schematic diagram showing the transmission routes of both westward-propagating equatorial and β-refracted Rossby waves.

Acknowledgments

Yi-Chen Cheng and Yu-Yu Yeh helped plot the bathymetry chart and wavenumber-frequency spectrum, respectively. To NAMRIA Administrator Peter N. Tiangco for the hourly coastal sea level data products. This work was supported by the National Science and Technology Council (NSC) of Taiwan. SJ is sponsored under grant NSC-111-2611-M-002-020,

NSC-111-2119-M-002-014, and NSTC-112-2119-M-002-023. MEDM is sponsored under grant NSTC-112-2119-M-002 -023. TYH is sponsored by the NSTC.

Data Availability Statement

Satellite SLA is obtained from CMEMS (accessible at https://doi.org/10.48670/moi-00148). Sea level records from tide gauge stations in Palawan is available at https://doi.org/10.5281/zenodo.10396727.

References

Anderson, D. L. T., Bryan, K., Gill, A. E., & Pacanowski, R. C. (1979). The transient response of the North Atlantic: Some model studies. *Journal of Geophysical Research*, *84*(C8), 4795. https://doi.org/10.1029/JC084iC08p04795

Anderson, D. L. T., & Gill, A. E. (1975). Spin-up of a stratified ocean, with applications to upwelling. *Deep Sea Research and Oceanographic Abstracts*, *22*(9), 583–596. https://doi.org/10.1016/0011-7471(75)90046-7

Cabanes, C., Huck, T., & Colin de Verdière, A. (2006). Contributions of Wind Forcing and Surface Heating to Interannual Sea Level Variations in the Atlantic Ocean. *Journal of Physical Oceanography*, *36*(9), 1739–1750. https://doi.org/10.1175/JPO2935.1

Cabrera, O. C., Villanoy, C. L., David, L. T., & Gordon, A. L. (2011). Barrier layer control of entrainment and Upwellingin the Bohol Sea, Philippines. *Oceanography*, *24*(1), 130–141. https://doi.org/10.5670/oceanog.2011.10

Calafat, F. M., Wahl, T., Lindsten, F., Williams, J., & Frajka-Williams, E. (2018). Coherent modulation of the sea-level annual cycle in the United States by Atlantic Rossby waves. *Nature Communications*, *9*(1). https://doi.org/10.1038/s41467-018-04898-y

Chelton, D. B., deSzoeke, R. A., Schlax, M. G., El Naggar, K., & Siwertz, N. (1998). Geographical Variability of the First Baroclinic Rossby Radius of Deformation. *Journal of Physical Oceanography*, *28*(3), 433–460. https://doi.org/10.1175/1520-0485(1998)028<0433:GVOTFB>2.0.CO;2

Chelton, D. B., & Schlax, M. G. (1996). Global Observations of Oceanic Rossby Waves. *Science*, *272*(5259), 234–238. https://doi.org/10.1126/science.272.5259.234

Cushman-Roisin, B., & Beckers, J.-M. (2011). Chapter 9 - Barotropic waves, in International Geophysics, edited by B. Cushman-Roisin and J.-M. Beckers, pp. 271–315, Academic Press, https://doi.org/10.1016/B978-0-12-088759-0.00009-2.

Delcroix, T., Picaut, J., & Eldin, G. (1991). Equatorial Kelvin and Rossby waves evidenced in the Pacific Ocean through Geosat sea level and surface current anomalies. *Journal of Geophysical Research*, *96*(S01), 3249. https://doi.org/10.1029/90JC01758

du Penhoat, Y., & Cane, M. A. (1991). Effect of low-latitude western boundary gaps on the reflection of equatorial motions. *Journal of Geophysical Research*, *96*(S01), 3307. https://doi.org/10.1029/90jc01798

Foreman, M.G.G. (1977). Manual for tidal heights analysis and prediction. *Pacific Marine Science Report 77-10*, Institute of Ocean Sciences, Patricia Bay, Sidney, British Columbia.

Foreman, M.G.G. (1978). Manual for tidal currents analysis and prediction. *Pacific Marine Science Report 78-6*, Institute of Ocean Sciences, Patricia Bay, Sidney, British Columbia.

Fu, L.-L., Vazquez, J., & Perigaud, C. (1991). Fitting Dynamic Models to the Geosat Sea Level Observations in the Tropical Pacific Ocean. Part I: A Free Wave Model. *Journal of Physical Oceanography*, *21*(6), 798–809. https://doi.org/10.1175/1520-0485(1991)021<0798:FDMTTG>2.0.CO;2

Godin, G. (1991). The analysis of tides and currents. In: Parker, B.B. (Ed.), Tidal Hydrodynamics. New York: Wiley.

Jacobs, G. A., Emery, W. J., & Born, G. H. (1993). Rossby Waves in the Pacific Ocean Extracted from Geosat Altimeter Data. *Journal of Physical Oceanography*, *23*(6), 1155–1175. https://doi.org/10.1175/1520-0485(1993)023<1155:RWITPO>2.0.CO;2

Jacobs, G. A., Hurlburt, H. E., Kindle, J. C., Metzger, E. J., Mitchell, J. L., Teague, W. J., & Wallcraft, A. J. (1994). Decade-scale trans-Pacific propagation and warming effects of an El Niño anomaly. *Nature*, *370*(6488), 360–363. https://doi.org/10.1038/370360a0

Jan, S., Chang, M. H., Yang, Y. J., Sui, C. H., Cheng, Y. H., Yeh, Y. Y., & Lee, C. W. (2021). Mooring observed intraseasonal oscillations in the central South China Sea during summer monsoon season. *Scientific Reports*, *11*(1). https://doi.org/10.1038/s41598-021-93219-3

Kessler, W. S. (1990). Observations of long Rossby waves in the northern tropical Pacific. *Journal of Geophysical Research*, *95*(C4), 5183–5217. https://doi.org/10.1029/JC095iC04p05183

Matsuno, T. (1966). Quasi-Geostrophic Motions in the Equatorial Area. *Journal of the Meteorological Society of Japan. Ser. II*, *44*(1), 25–43. https://doi.org/10.2151/jmsj1965.44.1_25

McCreary, J. (1976). Eastern Tropical Ocean Response to Changing Wind Systems: with Application to El Niño. *Journal of Physical Oceanography*, *6*(5), 632–645. https://doi.org/10.1175/1520-0485(1976)006<0632:ETORTC>2.0.CO;2

Meyers, G. (1979). Annual Variation in the Slope of the 14°C Isotherm along the Equator in the Pacific Ocean. *Journal of Physical Oceanography*, *9*(5), 885–891. https://doi.org/10.1175/1520-0485(1979)009<0885:AVITSO>2.0.CO;2

Meyers, S. D., Liu, M., O'Brien, J. J., Johnson, M. A., & Spiesberger, J. L. (1996). Interdecadal Variability in a Numerical Model of the Northeast Pacific Ocean: 1970–89. *Journal of Physical Oceanography*, *26*(12), 2635–2652. https://doi.org/10.1175/1520-0485(1996)026<2635:IVIANM>2.0.CO;2

National Oceanic and Atmospheric Administration, National Weather Service, Climate Prediction Center. (2023). Cold and warm episodes by season. Retrieved from https://origin.cpc.ncep.noaa.gov/products/analysis_monitoring/ensostuff/ONI_v5.php

Pawlowicz, R., Beardsley, B., & Lentz, S. (2002). Classical tidal harmonic analysis including error estimates in MATLAB using T_TIDE. *Computers & Geosciences*, *28*(8), 929–937. https://doi.org/10.1016/S0098-3004(02)00013-4

Piecuch, C. G., & Ponte, R. M. (2012). Buoyancy-driven interannual sea level changes in the southeast tropical Pacific. *Geophysical Research Letters*, *39*(5). https://doi.org/10.1029/2012GL051130

Qiu, B. (2003). Kuroshio Extension Variability and Forcing of the Pacific Decadal Oscillations: Responses and Potential Feedback. *Journal of Physical Oceanography*, *33*(12), 2465–2482. https://doi.org/10.1175/2459.1

Sirven, J., Mignot, J., & Crépon, M. (2019). Generation of Rossby waves off the Cape Verde Peninsula: The role of the coastline. *Ocean Science*, *15*(6), 1667–1690. https://doi.org/10.5194/os-15-1667-2019

Spall, M. A., & Pedlosky, J. (2005). Reflection and Transmission of Equatorial Rossby Waves*. *Journal of Physical Oceanography*, *35*(3), 363–373. https://doi.org/10.1175/JPO-2691.1

Stammer, D., Park, S., Köhl, A., Lukas, R., & Santiago-Mandujano, F. (2008). Causes for large-scale hydrographic changes at the Hawaii Ocean time series station. *Journal of Physical Oceanography*, *38*(9), 1931–1948. https://doi.org/10.1175/2008JPO3751.1

Torrence, C., & Compo, G. P. (1998). A Practical Guide to Wavelet Analysis. *Bulletin of the American Meteorological Society*, *79*(1), 61–78. https://doi.org/10.1175/1520-0477(1998)079<0061:APGTWA>2.0.CO;2

Uz, B. M., Yoder, J. A., & Osychny, V. (2001). Pumping of nutrients to ocean surface waters by the action of propagating planetary waves. *Nature*, *409*(6820), 597–600. https://doi.org/10.1038/35054527

Villanoy, C. L., Cabrera, O. C., Yñiguez, A., Camoying, M., de Guzman, A., David, L. T., & Lament, P. F. (2011). Monsoon-driven coastal upwelling off Zamboanga peninsula, Philippines. *Oceanography*, *24*(1), 156–165. https://doi.org/10.5670/oceanog.2011.12

White, W. B. (2000). Tropical Coupled Rossby Waves in the Pacific Ocean–Atmosphere System. *Journal of Physical Oceanography*, *30*(6), 1245–1264. https://doi.org/10.1175/1520-0485(2000)030<1245:TCRWIT>2.0.CO;2

White, W. B., Chao, Y., & Tai, C.-K. (1998). Coupling of Biennial Oceanic Rossby Waves with the Overlying Atmosphere in the Pacific Basin. *Journal of Physical Oceanography*, *28*(6), 1236–1251. https://doi.org/10.1175/1520-0485(1998)028<1236:COBORW>2.0.CO;2

Zang, X., Fu, L. L., & Wunsch, C. (2002). Observed reflectivity of the western boundary of the equatorial Pacific Ocean. *Journal of Geophysical Research: Oceans*, *107*(10). https://doi.org/10.1029/2000jc000719